Hindawi
Advances in Civil Engineering
Volume 2023, Article ID 6636781, 22 pages
https://doi.org/10.1155/2023/6636781

Research Article

Seismic Performance of Precast Concrete Column-to-Column Joint Using the Steel Plate Hoop and Bolts Connection

Dawei Yuan,[1,2] **Qi Shang**,[1] **Chun Han**,[3] **Jianpeng Sun**,[2] **and Qingning Li**[2]

[1]*School of Civil Engineering and architecture, Xinxiang University, Xinxiang 453003, China*
[2]*School of Civil Engineering, Xi'an University of Architecture and Technology, Xi'an 710055, China*
[3]*School of Civil Engineering and architecture, Xinxiang University, XAUAT Engineering Technology Co. Ltd., Xinxiang 453003, China*

Correspondence should be addressed to Dawei Yuan; 517461666@qq.com

Received 11 February 2023; Revised 2 July 2023; Accepted 3 July 2023; Published 24 July 2023

Academic Editor: Fadzli Mohamed Nazri

The traditional precast concrete column-to-column connections are widely used in the prefabricated concrete frame structures in China. However, many studies on the column-to-column joints have demonstrated their complex forms and poor construction efficiency. To overcome these shortcomings, a new type column–column connection with steel plate hoop and bolts was designed and proposed. In order to reveal the seismic performance of this new type connection, four precast concrete columns and two cast-in-situ columns were tested by cyclic lateral loading. They were compared and analyzed from the aspects of test phenomenon, failure mode, load–displacement relationship, strength, and stiffness degradation. The results showed that the prefabricated columns with this new type connection had the same seismic performance as the cast-in-place columns. Additionally, the strain curves of longitudinal reinforcement, stirrups, and steel plate hoops were presented, and the force transmission mode of this novel connection was analyzed. The results indicated that the innovative connection had reliable force transmission mode, which can provide reference for the application of prefabricated frame structure in the earthquake area.

1. Introduction

The seismic capacity of the precast concrete connection plays a key role in the earthquake of prefabricated concrete buildings. This point of view has been repeatedly confirmed, such as 1994 Northridge earthquake in the United States [1], 2008 Wenchuan earthquake in China [2], 2011 Van earthquake in Turkey [3], and so on.

Many studies have been carried out in order to improve the seismic performance of prefabricated concrete structure connections. The United States and Japan jointly carried out a research project on Precast Seismic Structural Systems (PRESS), and systematically studied the connections and seismic performance of precast concrete buildings [4]. From 2011 to 2017, the Chinese Academy of Building Research (CABR) had carried out the research on the National Science and Technology Support Project of "Research and Demonstration of New Prefabricated Concrete Building Technology" [5].

Although the above research projects had promoted the rapid development of precast concrete connection technology, these technologies are mainly wet connection technology [6], such as grout sleeve splicing for reinforcement [7, 8] and insertion connection [9] and grouting–anchoring connection [10, 11]. These column-to-column connections have good mechanical ability, but they have some shortcomings, such as complex construction procedures and slow construction speed [12, 13], which are restricting the development of assembled concrete structures.

Compared with wet connection, dry connection has the advantages of relatively simple structure and faster construction speed [5]. However, the dry connection is generally weaker than wet connection in terms of seismic performance and monolithic behavior [14]. So, the dry connection is

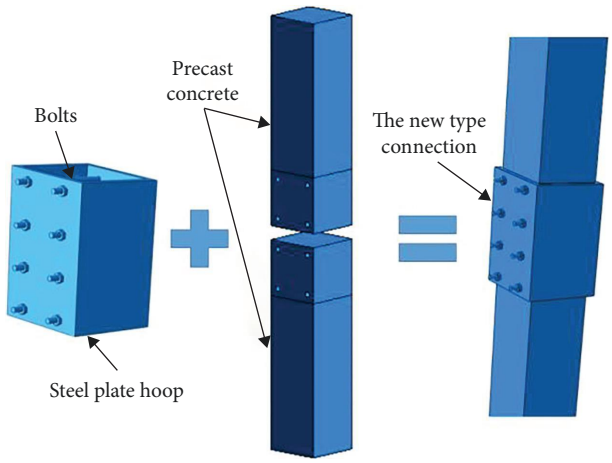

FIGURE 1: The steel plate hoop and bolts connection.

mostly used in nonearthquake area. There are few studies on the seismic performance of dry connections, and most of them focus on beam-to-column connections and shear wall connections, such as typical steel plate beam-to-column connection [15], steel plate beam-to-column connection [16], and so on. There are few studies on the seismic performance of column-to-column dry connections.

The new type column-to-column connection is proposed in this paper, as shown in Figure 1. This connection mode has a unique way to transfer the force. First, it is different from the traditional grout sleeve connection [7] because the longitudinal reinforcement between the two precast concrete elements is not connected. Second, this connection is also different from the concrete-filled steel tube (CFST) column. The concrete members and steel pipes are subjected to force together as a whole in CFST structures [17], while in new type connection, the force is transmitted from the concrete components to the steel tube. Therefore, it is necessary to study the seismic performance of this kind connection, and this can provide necessary evidence for this connection application in seismic areas.

2. Experimental Program

2.1. Specimen Design. Six test pieces were designed in order to find out that the prefabricated columns with this new type connection had the same seismic capacity as the cast-in-situ columns. The four prefabricated columns (W02, W03, Y01, and Y02) were using steel tube with bolts connection, and two cast-in-situ columns (W01 and C01) were the controlled specimens. Two axial load ratios were designed to study the seismic behavior of this connection method. The axial load ratio of W01, W02, W03, and Y01 was 0.6, and the axial load ratio of C01 and Y02 was 0.2. The length of the steel tube in W02 and W03 was 1,290 mm, but the thickness of the steel tube was different. The length of the steel tube in Y01 and Y02 was 890 mm, but axial load ratio was different. The details of all specimens were shown in Figure 2 and Table 1.

2.2. Specimen Preparation. The production process of specimens was shown in Figure 3. The reinforcement skeleton adopted rectangular spiral stirrup. Two *U*-shaped steel plates were welded into a rectangular steel tube. The end of the longitudinal reinforcement adopted 90° right angle hook, and the hook length was 120 mm. All the specimens were cast with concrete.

2.3. Material Properties. The mechanical properties of longitudinal reinforcement, stirrup, bolts, and steel tubes were tested according to Standard for Test Method of Mechanical Properties on Ordinary Concrete [18]. The test results were shown in Table 2. According to Test Method of Mechanical Properties on Ordinary Concrete [19], the average concrete compressive strength (f_c), obtained by testing three 150 mm × 150 mm × 150 mm cubes, was 43.7 MPa. Besides, the compressive strength of filling grout, obtained by testing three 150 mm × 150 mm × 150 mm cubes, is 51.0 MPa.

2.4. Test Setup and Loading History. The cyclic loading history was adopted according to the code JGJ 101-2015 [20], as shown in Figure 4. The axial force on the top of column was generated by the 500 T hydraulic jack, and the low cycle lateral loading at the top of the column was generated by MTS actuator of 100 T.

According to code for seismic design of buildings [21], the maximum limit value of the axial load ratio was 0.6 in reinforced concrete frame structure columns. Therefore, the upper limit of the axial load ratio selected was 0.6 in this paper. The axial load ratio of 0.2 was chosen because it was the lower limit value in the design of RC frame columns. So, the axial load with $0.6f_c \cdot A_g$ (480 kN) and $0.2f_c \cdot A_g$ (160 kN) was applied, where A_g was the gross area of the column cross-section, and f_c was the average compressive strength of concrete acquired from the cube test. The constant axial load during the lateral loading was kept constant.

Before the specimens yielded, the lateral loading was force controlled, and one cycle was performed at each force level. The estimated lateral load of each stage was 50 kN. After reaching the yield displacement, it was changed to displacement control. Each cycle was repeated thrice. When the load fell below 85% of the ultimate load, the specimen was considered to be failed and the loading was stopped. The loading history was shown in Figure 5.

2.5. Installed Test Points. In order to understand the mechanical behavior of the new type connection under the combined action of compression–bending–shear, some strain gauges were installed on the specific locations, as shown in Figure 6. Strain gauges were installed on the longitudinal bars and stirrups at the positions of section 1-1, section 2-2, and section 3-3, respectively. The strain gauges of No. 4, No. 5, and No. 6 were installed on the steel plate hoop, as shown in Figures 6(b) and 6(c). In order to measure the strain of the bolts, strain gauges of No. 7, No. 8, No. 9, and No. 10 were placed at the midpoint of the bolt, respectively. In addition, the displacement meter at the position used to measure is

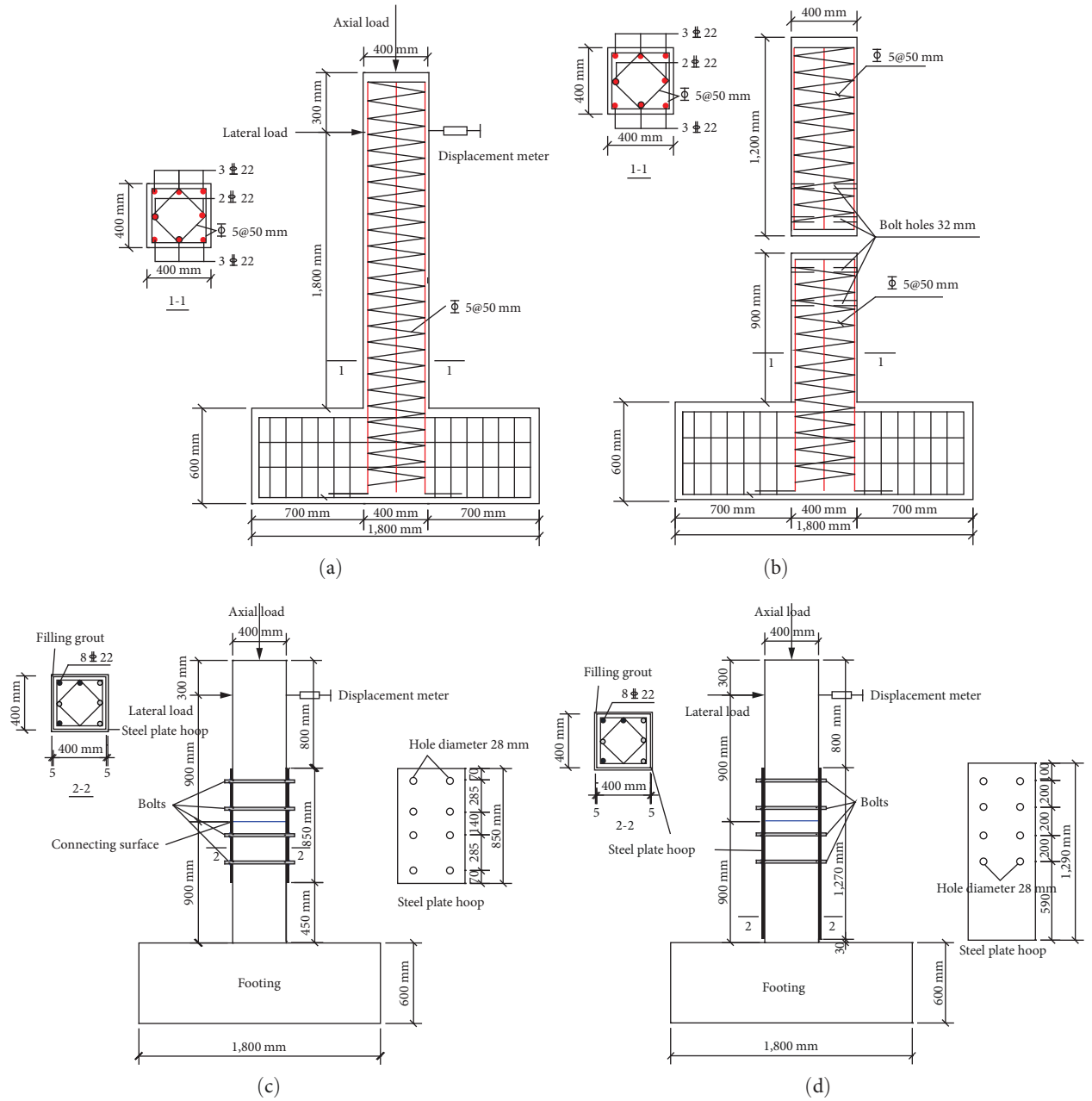

Figure 2: Specific size and structure of specimen: (a) size and reinforcement of W01 and C01; (b) size and reinforcement of prefabricated columns; (c) size and reinforcement of W02 and W03; (d) size and reinforcement of Y01 and Y02.

Table 1: Details of specimens.

Specimen	Section size (mm × mm)	Strength of concrete (MPa)	Longitudinal reinforcement	Stirrup spacing (mm)	Length of steel tube (mm)	Actual measured thickness of steel tube (mm)	Axial compressive load ratio
W01	400 × 400	C40	8Φ22	50	–	–	0.6
W02					1,290	5	0.6
W03					1,290	8	0.6
Y01					850	5	0.6
Y02					850	5	0.2
C01					–	–	0.2

Figure 3: Specimen preparation: (a) spiral stirrup; (b) steel plate hoop; (c) reinforcement skeleton; (d) precast concrete.

Table 2: Mechanical properties of steel.

Type	Steel category	Yield strength f_y (MPa)	Ultimate strength f_u (MPa)	Ultimate strength f_v (MPa)	Yield strain ε_y (10^{-6})
Steel plate hoop (5 and 8 mm)	Q235	320	475	200	1,524
Longitudinal reinforcement	C22 HRB400	450	660	320	2,250
Bolts	C22 HRB400				
Stirrup	Φ5 HRB400	1,050	1,170	–	5,250

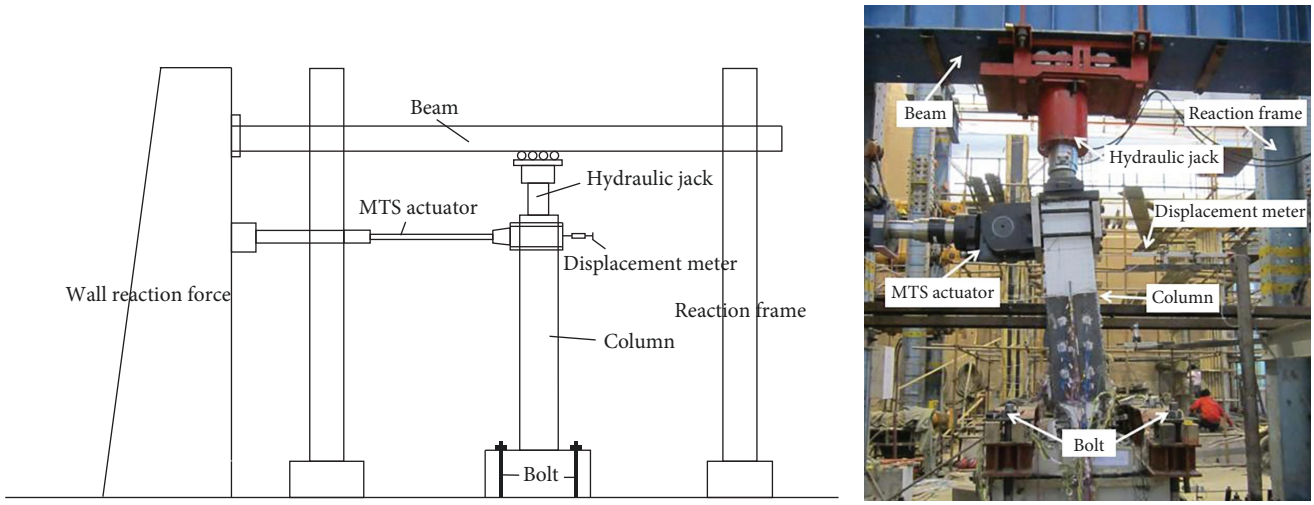

Figure 4: Schematic view of the loading device: (a) schematic test diagram; (b) actual test diagram.

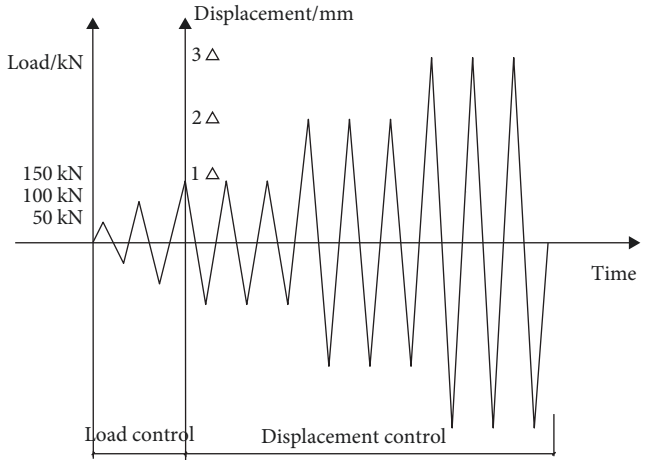

Figure 5: Loading history.

shown in Figure 2(a) and Figure 4. All test data were collected by TDS602 data acquisition instrument.

3. Experimental Results and Discussion

3.1. Failure Modes. The six test columns were finally failed by bending. The cast-in-situ columns (W01 and C01) and the prefabricated columns (Y01 and Y02) had obvious failure patterns at the column foot, such as cover concrete spalling and longitudinal reinforcement bending. However, the concrete spalling and longitudinal reinforcement bending were not found at the bottom of the prefabricated columns (W02 and W03), which may be due to the wrapping of steel plate hoops. The final failure state of each specimen was shown in Figures 7 and 8.

3.1.1. Test Process and Phenomenon of the Axial Load Ratio (0.6) Columns.
(1) Load Control Stage (*Lateral Load 0–250 kN*). In the load control stage, the specimens were at the elastic stage before the concrete cracks, and its loading and unloading curves were basically in coincidence for a line. When the lateral load reached about 200 kN, the first horizontal crack appeared in W01 and Y01. When the first horizontal crack occurred in W02 and W03, the lateral load reached about 250 kN.

(2) Displacement Control Stage (*Lateral Displacement 20–100 mm*). The penetrating cracks of columns W01 and Y01 gradually increased, and the width of the cracks increased continuously in the first cyclic lateral displacement (20 mm). Dense cracks occurred and developed in the end of the columns. When the lateral displacement of W01 reached about 40 mm and Y01 reached about 44 mm, the cover concrete of the column end in the compression area starts to crush locally and externally. When the lateral displacement of W01 reached about 90 mm and Y01 reached about 100 mm, the longitudinal reinforcement at the bottom of the column was failed by compression buckling.

The test columns of W02 and W03 had no tearing or buckling failure of the steel plate hoop during the whole loading process. There was a small amount of concrete peeling at the bottom of the columns, but after removing the steel plate hoop, the concrete inside was in good condition and no crushing phenomenon occurs.

3.1.2. Test Process and Phenomenon of the Axial Load Ratio (0.2) Columns.
(1) Load Control Stage (*Horizontal Load 0–150 kN*). When the lateral load of C01 and Y02 reached about 100 kN, the first horizontal crack appeared. With the increase of horizontal load, horizontal cracks increased continuously. After 150 kN, the sloping cracks appeared on the other side of the test columns.

(2) Displacement Control Stage (*Horizontal Displacement About 20–110 mm*). When the horizontal displacement reached about 30 mm, the concrete began to fell off at the bottom of the columns C01 and Y02. When the horizontal displacement reached 100 mm, the bottom concrete fell off completely. The longitudinal reinforcement and stirrup were

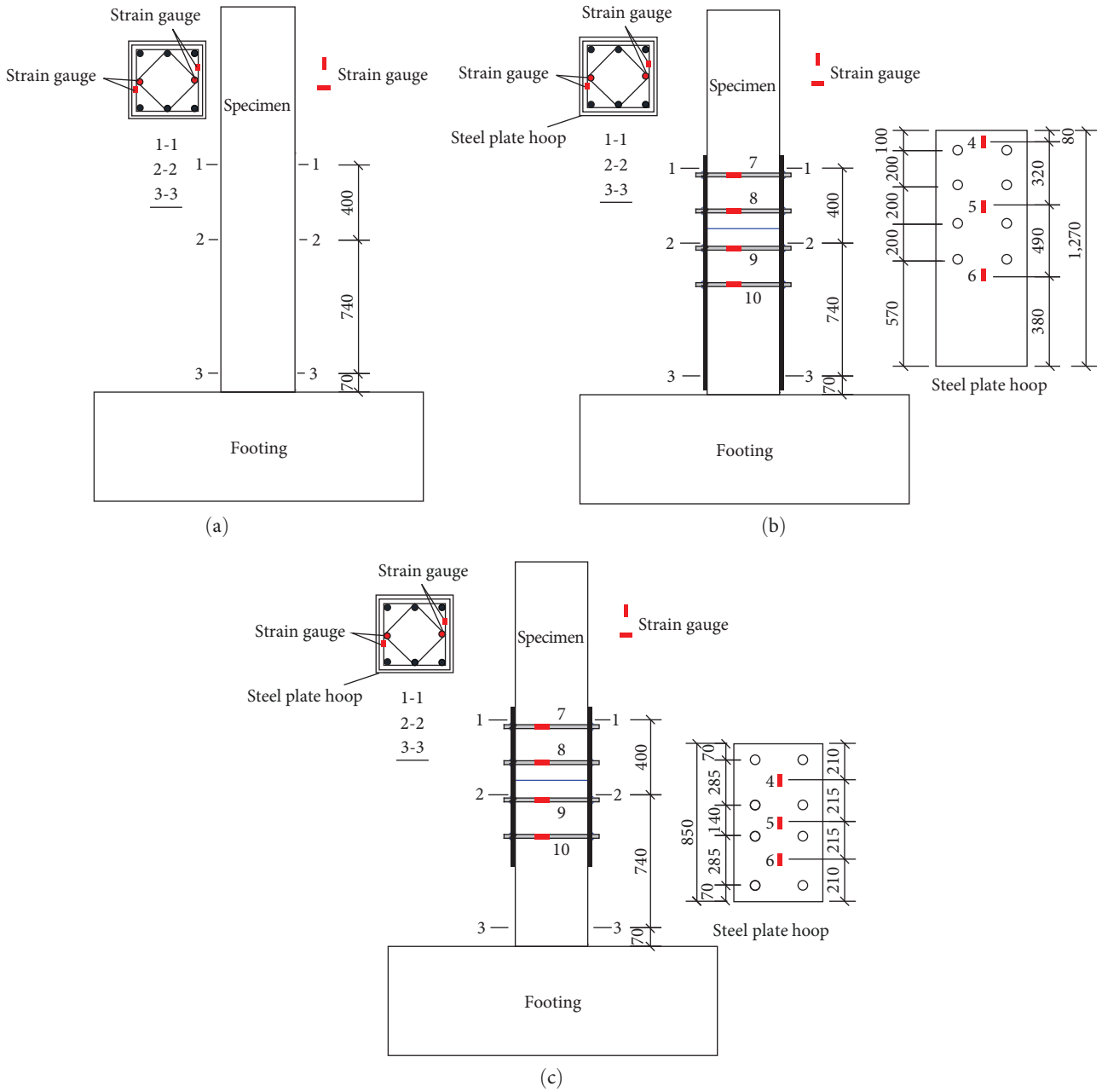

Figure 6: Strain gauge installation layout: (a) the position of strain gauges in W01 and C01; (b) the position of strain gauges in W02 and W03; (c) the position of strain gauges in Y01 and Y02.

all leak out, but the compression and buckling of the longitudinal reinforcement are not obvious, as shown in Figures 8(b) and 8(c).

In conclusion, the overall failure mode of the above six specimens belonged to bending moment failure, namely, the failure under large eccentric compression. Although W02 and W03 did not have the phenomenon of concrete falling off, according to the strain test results and loading process of longitudinal reinforcement, these two specimens also belonged to bending moment failure.

In order to check that this new type connection can achieve the seismic capacity of "equivalent to cast-in-situ connection," it is necessary to ensure that the connection did not fail before the bending failure occurs at the bottom. So, the test results are in good agreement with the design results.

3.2. Hysteresis Curve and Backbone Curves

3.2.1. Hysteresis Curve. The lateral load–displacement curve is an important tool to study the seismic behavior of the structure, which can reflect the ductility, stiffness degradation, and energy dissipation capacity of the specimens [22]. Figure 9 presents the hysteresis curve of all specimens. The horizontal displacements were collected by the TDS602 data acquisition instrument at the position of displacement meter (shown in Figure 4).

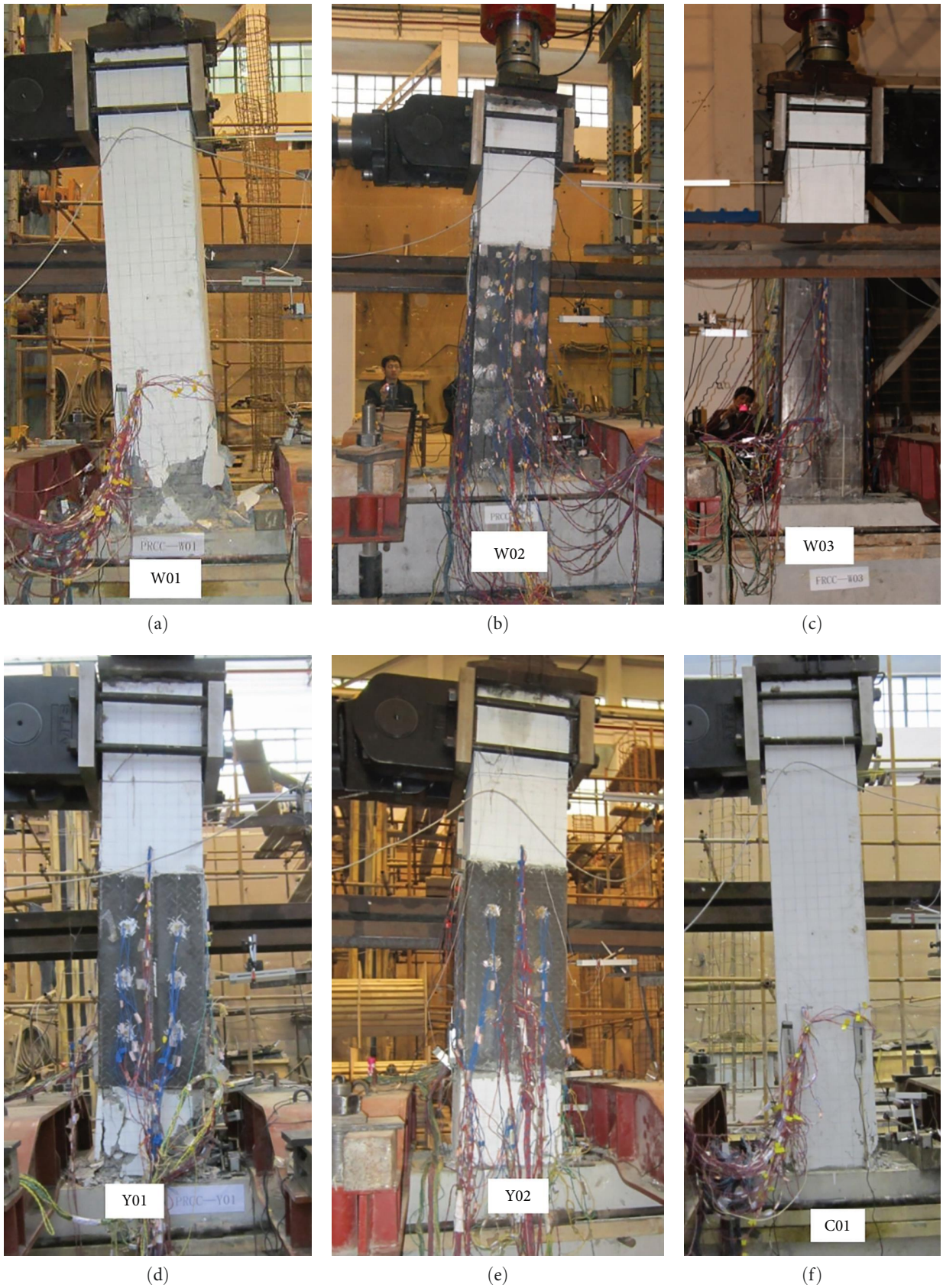

(a) (b) (c)

(d) (e) (f)

Figure 7: Loading diagram and failure modes: (a) W01; (b) W02; (c) W03; (d) Y01; (e) Y02; (f) C01.

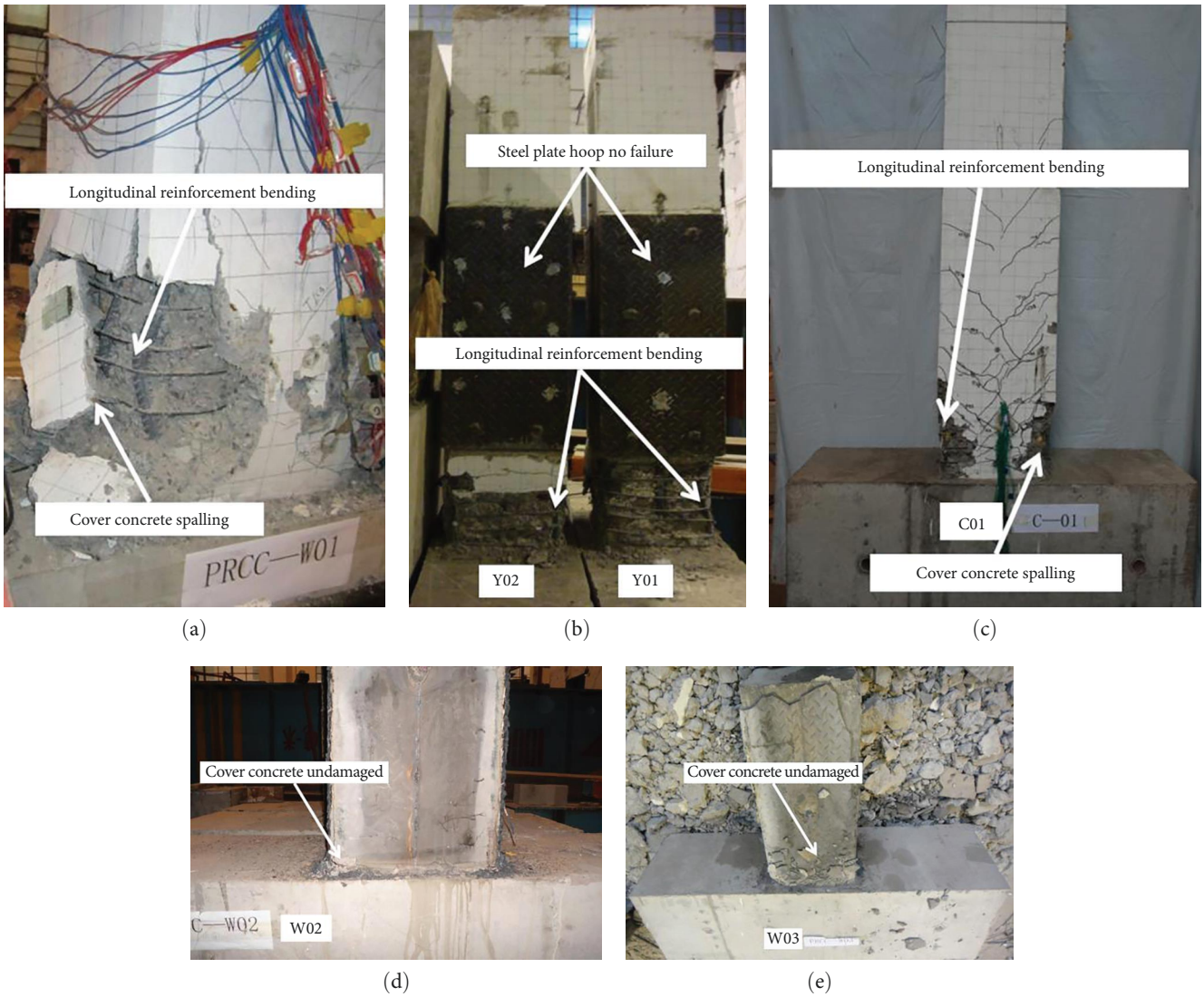

Figure 8: Failure modes: (a) W01; (b) Y01 and Y02; (c) C01; (d) W02; (e) W03.

It is observed that the shape curve of W01 and Y02 is similar, and the shape of C01 and Y02 is similar. Although the axial compression ratio of W02 and W03 is also 0.6, the shape of its hysteresis curve is not as plump as W01 and Y01. After the yield, the slope of the curves begins to shift, the range of the hysteresis loop enlarges gradually, and the energy dissipation increases gradually. At the same time, the bearing capacity and stiffness of the two displacement cycles are slightly lower than the first time. From the whole point of view, the hysteresis curve of all specimens is plump, and the prefabricated columns exhibit same seismic performance as the cast-in-situ columns.

3.2.2. Backbone Curves. The backbone curve is obtained by connecting the peak points of all the first cycles of the load–displacement in the cyclic loading test [23, 24]. Figure 10 shows the comparison of all specimens. Figure 10(a), on the left, shows the backbone curve of the measured specimens. Figure 10(b), on the right, shows the calculated dimensionless backbone curve. In the upper left corner, as shown in Figure 10(b), V and V_{max} represent the lateral load and the maximum lateral load in the loading process, respectively. We can better see the strength enhancement and degradation more easily at the same deformation through the dimensionless backbone curve.

We can observe the following characteristics of the backbone curve of the measured specimens. The peak strength of C01 and Y02 is obviously smaller than other specimens because of its axial compression ratio (0.2). The bearing capacity of all specimens after the peak load decreased, and there is a sharper decline phenomenon in W01 specimen than other prefabricated specimens. In the dimensionless backbone curve, the curve shape of prefabricated specimens is very similar, and the W01s curve is obviously sharp in the downward phase, indicating that this new type connection has better resistance to bearing capacity degradation decreased.

3.2.3. Strength and Ductility. The test results of each specimen for the yield strength P_y, peak strength P_k, ultimate strength P_u, yield lateral displacement Δ_y, peak lateral

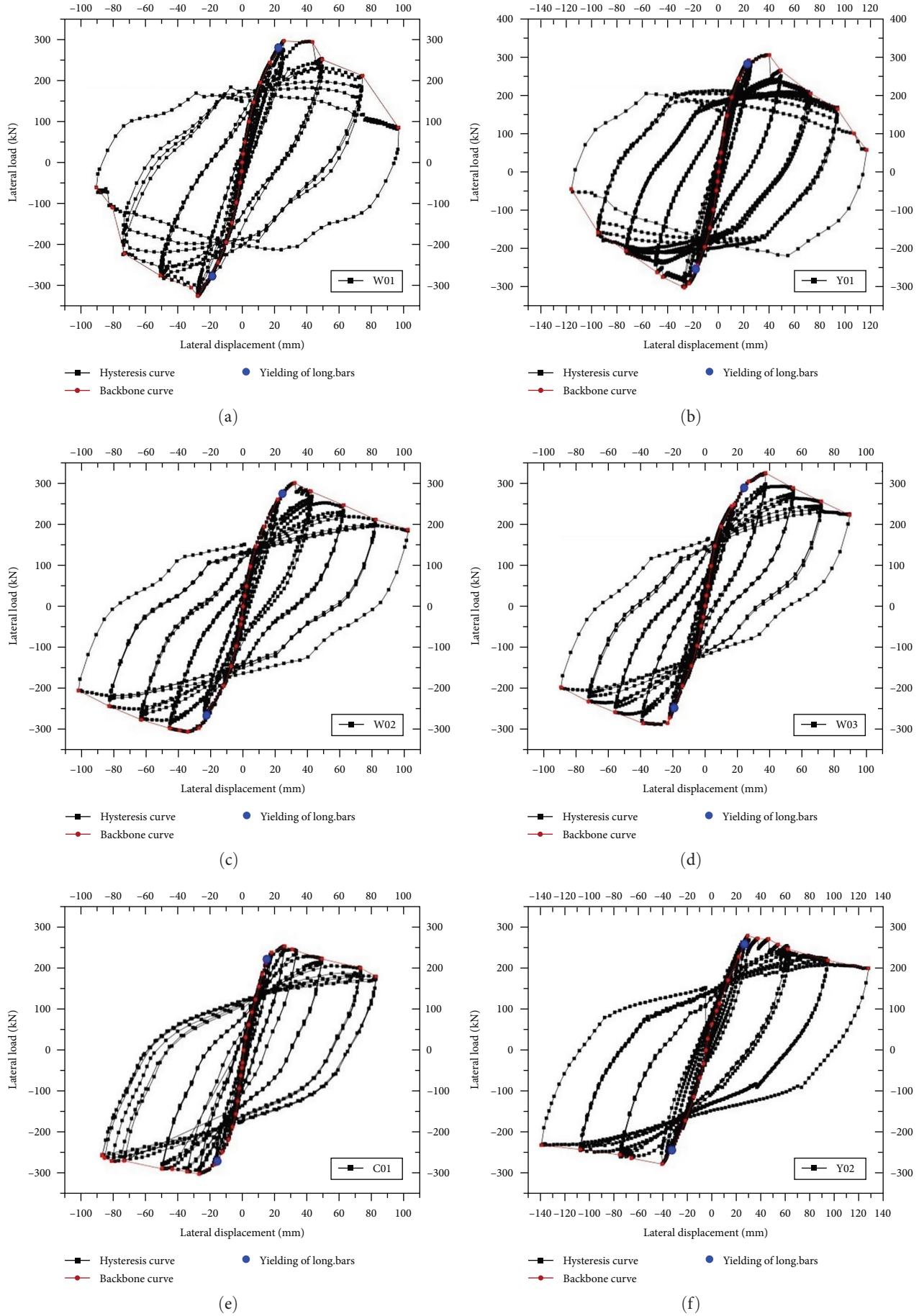

Figure 9: Lateral load–lateral displacement relationships of column specimens: (a) W01; (b) Y01; (c) W02; (d) W03; (e) C01; (f) Y02.

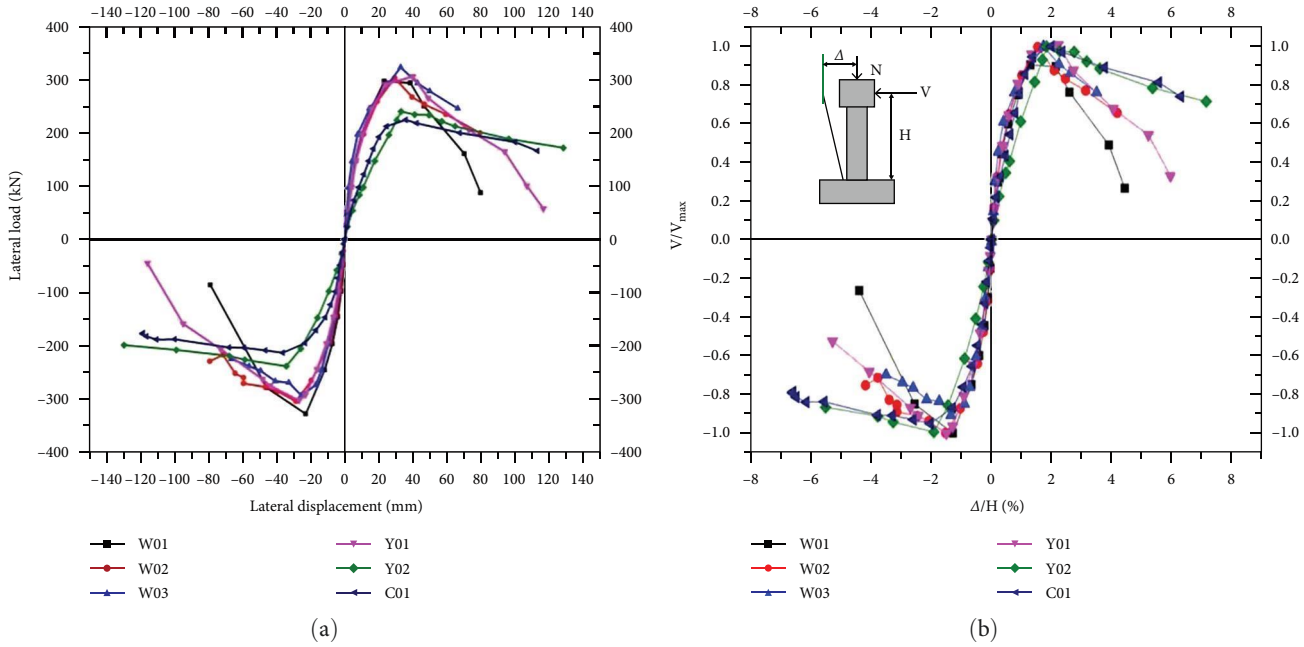

FIGURE 10: Backbone curves of the specimens: (a) the backbone curve; (b) the calculated dimensionless backbone curve.

TABLE 3: Ductility and energy dissipation capacity of the specimens.

Column ID		Yield strength and lateral displacement		Peak strength and lateral displacement		Ultimate strength and lateral displacement		Ductility ratio		Story drift	
		P_y/kN	Δ_y/mm	P_k/kN	Δ_k/mm	P_u/kN	Δ_u/mm	$\mu = \frac{\Delta_u}{\Delta_y}$		$\theta = \frac{\Delta_u}{H}$	
W01	Front	249.6	15.44	296.8	23.57	252.3	47.38	3.1	3.0	1/38	1/38
	Back	−281.5	−16.33	−326.6	−23.24	−277.6	−47.39	2.9		1/38	
W02	Front	254.0	17.83	302.2	29.60	256.8	55.26	3.1	3.7	1/33	1/30
	Back	−260.9	−16.32	−307.2	−28.91	−261.1	−70.15	4.3		1/26	
W03	Front	268.1	18.12	325.2	33.37	276.5	56.36	3.1	3.8	1/32	1/32
	Back	−248.8	−13.68	−289.6	−21.91	−246.2	−59.36	4.4		1/32	
Y-01	Front	262.51	18.97	305.9	40.02	260.02	51.25	2.7	2.7	1/35	1/36
	Back	−259.6	−18.63	−303.2	−27.02	−257.7	−48.48	2.6		1/37	
Y-02	Front	221.35	30.12	240.2	33.01	204.22	74.66	2.4	3.3	1/24	1/20
	Back	−211.7	−27.51	−238.7	−34.49	−202.3	−118.2	4.2		1/15	
C-01	Front	200.85	22.01	224.4	35.85	190.41	85.62	3.9	4.9	1/21	1/18
	Back	−180.5	−19.44	−213.3	−36.58	−181.1	−117.2	6.0		1/15	

displacement Δ_k, maximum lateral displacement Δ_u, displacement ductility ratio μ, and story drift θ are presented in Table 3. The positive values are in the direction of pull loading, and the negative values are in the direction of push loading. The relevant values of ductility ratio and ultimate interlayer displacement are listed in Table 3 [21]. The average values of displacement ductility ratio and ultimate story drift are calculated by Equations 1 and 2:

$$\mu = \frac{|\Delta_u^+| + |\Delta_u^-|}{|\Delta_y^+| + |\Delta_y^-|}, \tag{1}$$

$$\theta = \frac{|\Delta_u^+| + |\Delta_u^-|}{2H}, \tag{2}$$

where H is the height of the specimen ($H = 1{,}800$ mm). According to the code for seismic design of buildings, the interstory drift should be not less than 1/50, which is the limit value of reinforced concrete frame under the action of strong earthquakes (rare earthquakes) [25]. The ultimate story drifts of all specimens are more than 1/50, and the ultimate story drifts of all prefabricated specimens are more than the integral pouring specimen. It indicates that

this new type connection columns have good seismic deformation capacity and are superior to cast-in-situ column in deformation capacity.

3.2.4. Strength Degradation. The degradation coefficient of strength λ_i is an important reference contents in the evaluation of structural seismic performance, which can reflect the nonlinear characteristics of specimens under cyclic load and the change process of bearing capacity. The degradation coefficient of strength is defined as follows:

$$\lambda_i = \frac{F_j^i}{F_j^1}, \tag{3}$$

where F_j^i is the lateral load corresponding to the ith cycle peak point at the jth level of loading and F_j^1 is the lateral load corresponding to the first-cycle peak point at the jth level of loading. Figure 11 shows the strength degradation coefficient of each testing column and horizontal displacement of the relationship. We can observe the following conclusions:

(1) As the lateral displacement increases, the strength of each specimen constantly decays. As shown in Figure 11, the strength degradation value with the axial load ratio of 0.6 is greater than the columns with an axial load ratio of 0.2. This indicates that the strength degradation of the columns with larger axial load ratio is greater.

(2) When the axial load ratio is 0.6, the strength degradation of the W01 and Y01 is significantly greater than that of W02 and W03. Especially in the last displacement control, the strength degradation value of W01 is significantly reduced to below 0.8, while the strength degradation values of W02 and W03 are remained above 0.9. Generally, when the steel plate hoop increases and thickens, the internal failure of the component can be obviously improved, while the steel hoop of Y01 has no obvious improvement on the failure of the component. The strength degradation of C01 and Y02 is similar, which indicates that this new type of prefabricated connection has the same strength degradation ability as the cast-in-situ structure. The seismic capacity of the new connection columns is slightly higher than that of the cast-in-situ columns.

3.2.5. Stiffness Degradation. With increasing lateral displacement and number of cycles, the level of the specimens' failure continues to accumulate, resulting in stiffness degradation. This failure is manifested in the following aspects: the development of cracks, the yield of longitudinal steel bars and stirrups, and the crushing of concrete. The secant stiffness is used to represent the characteristics of the specimens, and the stiffness equation is obtained as follows:

$$k_i = \frac{|+F_i| + |-F_i|}{|+\Delta_i| + |-\Delta_i|}, \tag{4}$$

where Δ_i is the peak displacement in the ith cycle of a displacement-control loading protocol and F_i is the corresponding peak load in the ith cycle.

Figure 12 shows the variation of the stiffness degradation of all specimens with the lateral displacement, from which we can observe the following.

The stiffness degradation curves of the cast-in-situ columns (W01 and C01) and other prefabricated columns are similar. As the lateral displacement increases, the stiffness of all specimens are constantly decayed. When the displacement is less than 40 mm, the rate of stiffness degradation is fast, and when the displacement is greater than 50 mm, the rate of stiffness degradation degrades slowly. This indicates that assembled columns have similar stiffness degradation resistance to the cast-in-situ columns. The stiffness degradation of columns (W02 and W03) is larger than Y01, which indicates that the increase of steel tube thickness has little effect on stiffness degradation resistance.

3.3. Analysis of Strain Test Results

3.3.1. Strain Analysis of Stirrups. Figure 13 shows the relation curve between stirrup strain and lateral load at the sections 1-1, 2-2, and 3-3 of each specimen, and the position is shown in Figure 6. We can observe the following:

(1) As shown in Figure 13, the section 1-1 is at the top of the columns, and the stirrup strain values of all test columns are relatively close. The bending moment of section 1-1 is the smallest, so the strain value of the stirrups is the smallest.

(2) The section 2-2 is in the middle of the test columns, which is wrapped by steel plate hoop in the precast concrete columns. This position is also inside the connection, so the strain value of the stirrups is significant difference in all test columns. The stirrup strain of W02 and W03 specimens is slightly smaller than the cast-in-situ column W01, while the stirrup strain of Y01 and Y02 is significantly smaller than that of W02 and W03. This shows that the steel plate hoop and bolts share the stress by the stirrup in the process of force transfer.

(3) The stirrup strain at section 3-3 of all test columns is the largest because the section 3-3 is located at the bottom of the columns and bears the largest bending moment. The maximum value of stirrup strain in the specimens (W02 and W03) is obviously smaller than the specimens (W01 and Y01) without steel plate hoop. This shows that the steel plate hoop effectively limits the transverse deformation of concrete.

3.3.2. Strain Analysis of Longitudinal Reinforcements. Figure 14 shows the strain-lateral load curves of longitudinal reinforcements at sections 1-1, 2-2, and 3-3 in all test columns, from which we can observe the following:

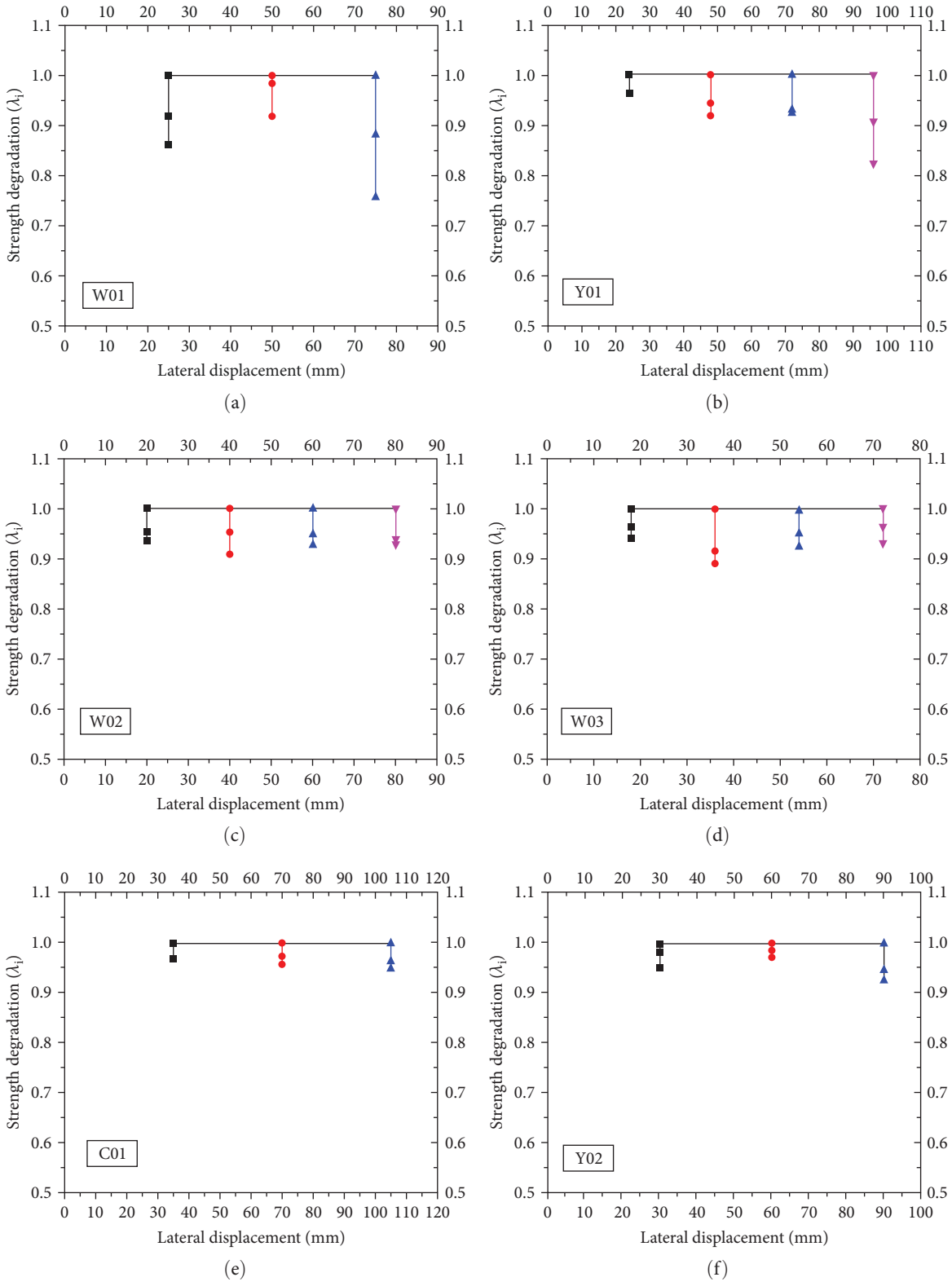

Figure 11: Comparisons of strength degradation: (a) W01; (b) Y01; (c) W02; (d) W03; (e) C01; (f) Y02.

(1) We can find that the shape of the blue curve is irregular, and this curve represents the strain of the longitudinal reinforcement at section 3-3 in all columns. This is mainly due to the tensile or buckling failure of the longitudinal reinforcement at the section 3-3 of all columns, resulting in the failure of the strain gauges.

(2) The red curve represents the strain of the longitudinal reinforcement at section 2-2, and this position is

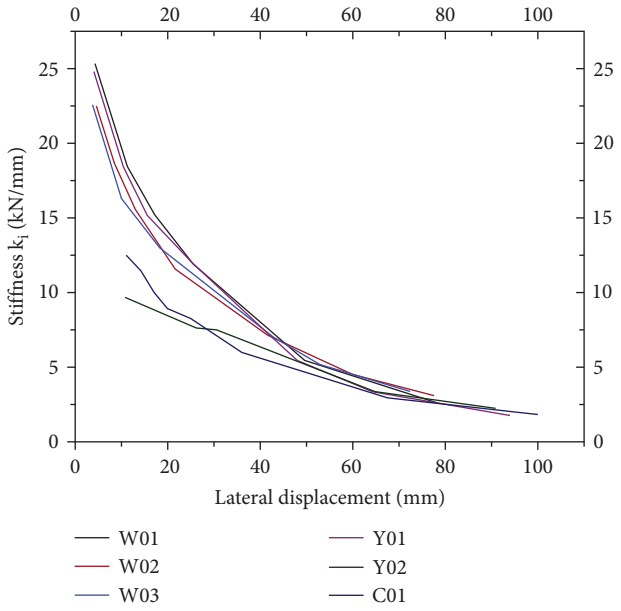

Figure 12: Comparisons of stiffness degradation.

wrapped in the steel plate hoop. The strain value of prefabricated columns is smaller than that of cast-in-situ columns at the same location, as shown in Figure 14. This shows that the steel plate hoops and bolts help the longitudinal reinforcement to bear a large amount of tensile stress during the process of force transfer.

(3) The black curve represents the strain of longitudinal reinforcement at section 1-1. The shape of this curve in all specimens is similar, which indicates that the tensile stress of longitudinal reinforcement of all test columns at this position is similar.

To sum up, the strain of longitudinal reinforcement at section 1-1 and section 3-3 is similar, while the strain at section 2-2 is different, which indicates that the new type connection can effectively transfer the tensile stress of longitudinal reinforcement.

3.3.3. Strain Analysis of Steel Hoop. Figure 15 shows the strain curve of the steel hoop at positions No. 4, No. 5, and No. 6. The specific position of the steel hoop is shown in Figure 4. The following conclusions can be obtained:

(1) The strain curves shape of columns W02 and W03 is similar, while the shape of Y01 and Y02 is similar. This is mainly because the specific positions No. 4, No. 5, and No. 6 are different. In W02 and W03 columns, the positions No. 4 and No. 6 are on the outside of the bolts, while in Y01 and Y02 specimens, the positions No. 4 and No. 6 are between the bolts.

(2) In the W02 and W03, the peak strain value of steel hoop at No. 5 position is the largest, and the peak strain value at No. 4 and No. 6 positions is small, while the peak strain value at No. 6 position is the largest. This shows that the No. 5 position on the tension side of the steel plate hoop bears the main tension, while the No. 4 and No. 6 positions hardly bear the tension. However, on the compression side of the steel plate hoop, the whole side has to bear the pressure. The more close to the column root, the greater pressure born by the steel plate hoop. This shows that the tensile force is gradually transferred from the longitudinal reinforcements to the steel plate hoop through the bolts.

(3) It is obvious that the strains of the steel hoop are far from the yield strain. On one hand, it is because the main function of the steel hoop is to transmit the bending moment, and the bending moment borne by the connection is not large; on the other hand, in order to ensure that the steel hoop does not yield and fail, the bearing capacity of the steel hoop has a certain redundancy.

3.3.4. Strain Analysis of Bolts. Figure 16 shows the strain curve of the bolts at positions No. 7, No. 8, No. 9, and No. 10. The specific position of the bolts is shown in Figure 4. The following conclusions can be obtained:

(1) All strain values are far below the yield strain of the bolts, as shown in Figure 16. The curve shape of W02 and W03 is similar. The peak strain of bolts No. 7 and No. 8 is larger than bolts No. 8 and No. 9.

(2) The peak strain value of W02 reaches 500, and the peak strain of W03 bolt is only 200, which indicates that increasing the thickness of the steel plate hoop can reduce the tensile force of the bolts. It is difficult to make a comparative analysis because the positions of bolts in Y01 and Y02 are different from W02 and W03.

(3) The tensile stress of bolts is small, and it plays a small role in limiting the transverse deformation of concrete. Therefore, the main function of the bolts is to limit the slip between the steel plate hoop and the precast concrete member.

4. Analysis and Calculation Methods of Mechanical Properties

Through the above strain analysis of stirrups, longitudinal reinforcements, steel plate hoops, and bolts at different positions, we can deduce the force transmission mode of the force on the new type connection.

4.1. Analysis of Failure Mode. Under the lateral load V, the relative movement trend is shown in Figure 17(a), and the diagram of axial, bending moment, and shear received by the test column is shown in Figure 17(b). According to the above internal force diagram, the following four possible failure modes can be obtained.

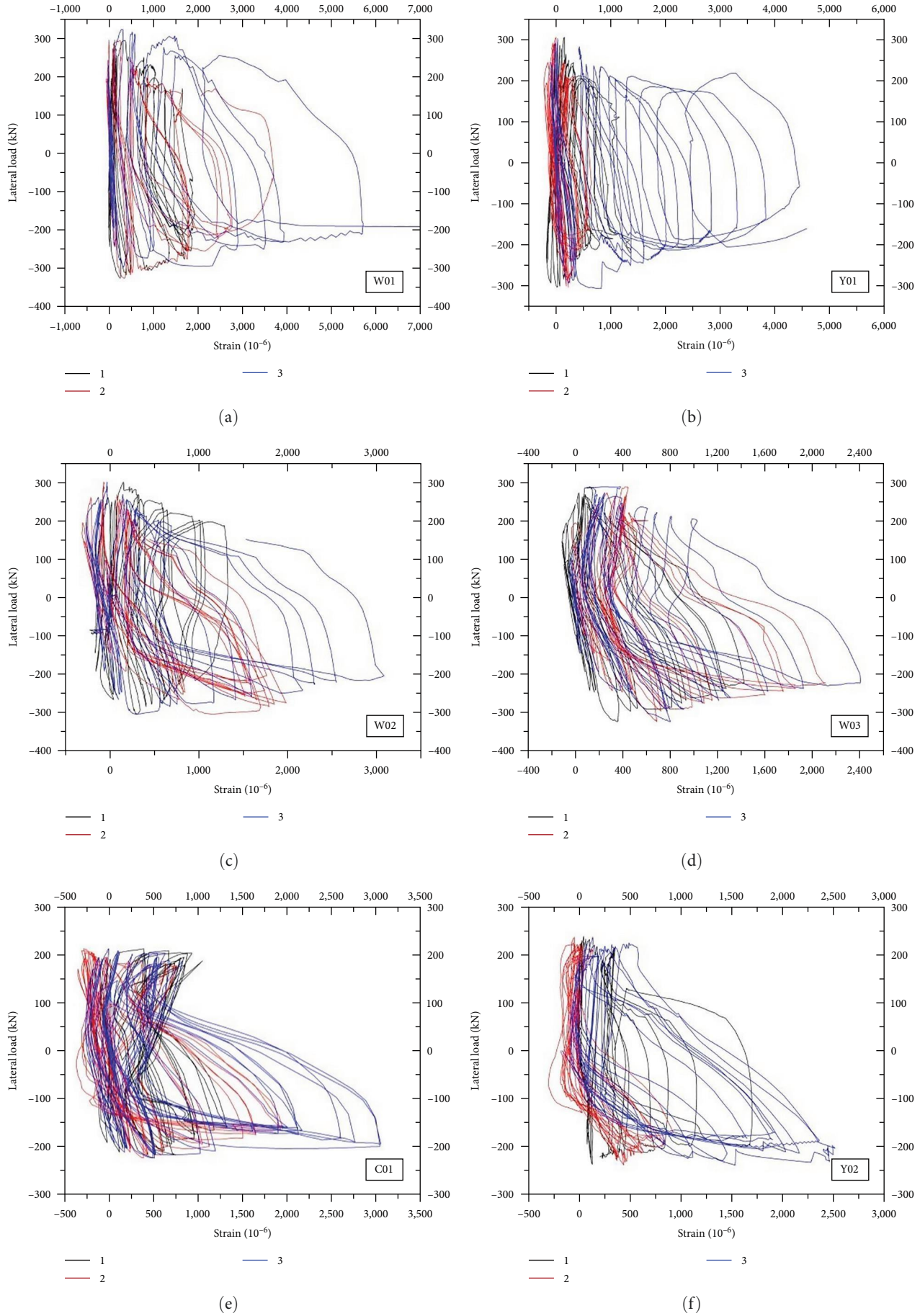

Figure 13: Strain curve of stirrup at positions 1, 2, and 3 in specimens: (a) W01; (b) Y01; (c) W02; (d) W03; (e) C01; (f) Y02.

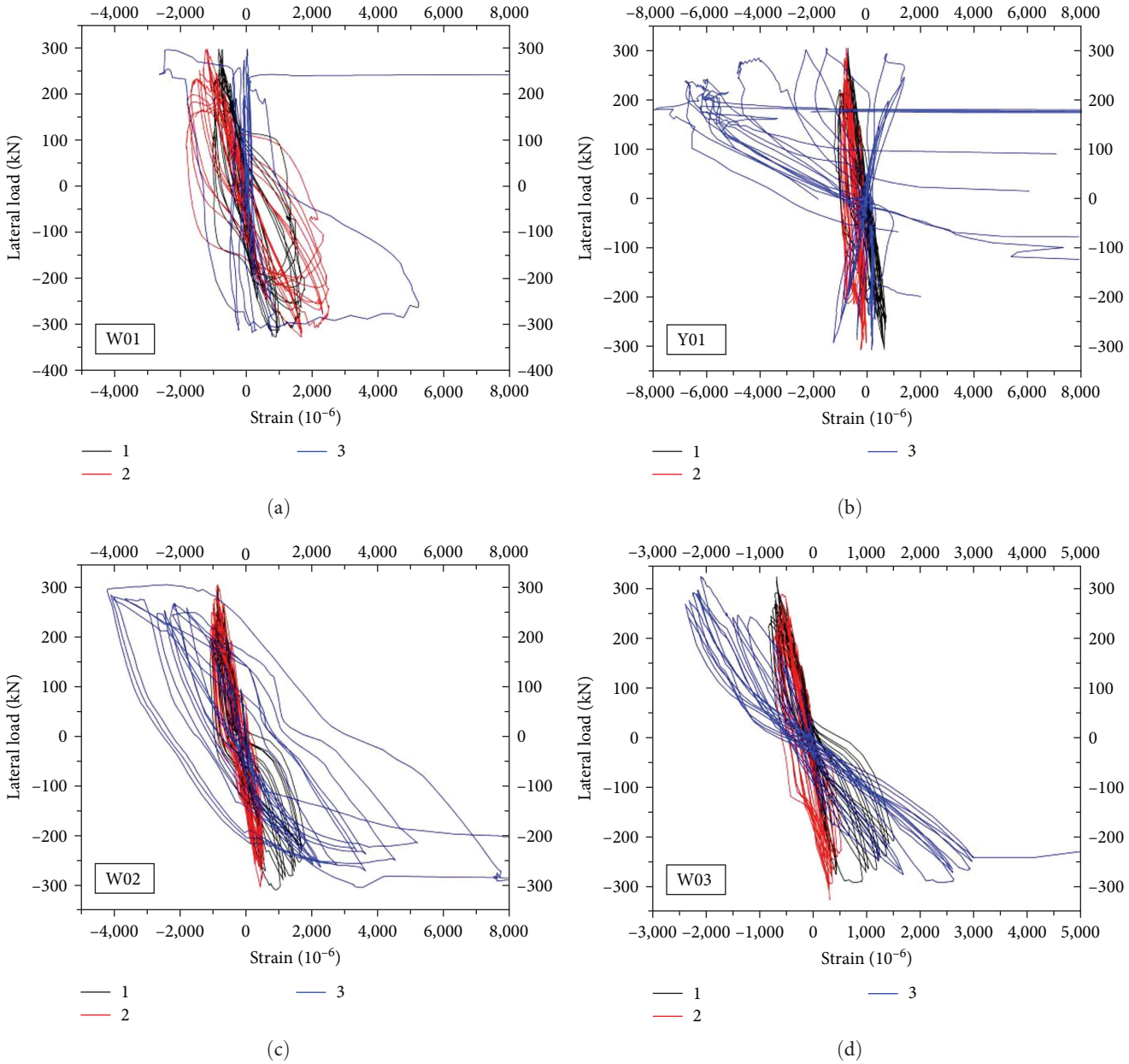

Figure 14: Continued.

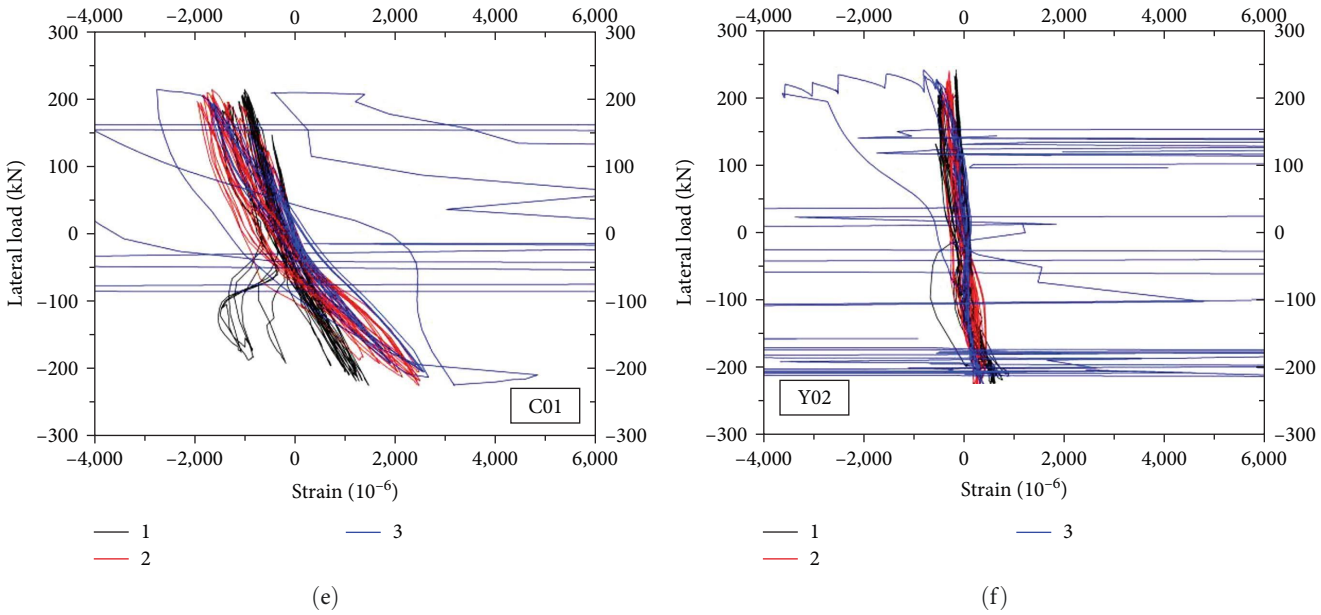

Figure 14: Strain curves of longitudinal reinforcement: (a) W01; (b) Y01; (c) W02; (d) W03; (e) C01; (f) Y02.

4.1.1. Bending Failure of Section 2-2. The section 2-2 is the seam of two precast concrete members, with weak connection and no longitudinal reinforcement passing through. Although the bending moment borne by this section is not the largest, the bending failure of CFST may occur. In order to ensure the reliability of the connection, this failure is not allowed.

4.1.2. Bending Failure of Section 3-3. This section 3-3 is at the bottom of the column and bears the maximum bending moment, so bending failure would occur. This destruction is allowed, which is also consistent with the experimental phenomenon.

4.1.3. Shear Failure of Bolts. In the process of bearing force, the connection node mainly plays the role of transferring the bending moment and shear force, and the bolts need to have sufficient shear strength and tensile strength. In order to ensure the reliability of the connection, this failure is also not allowed.

4.1.4. Tear Failure of Steel Plate Hoop. The steel plate hoop will produce cupping effect in the process of transferring bending moment, which may cause the steel plate hoop to tear. This failure is also not allowed.

In order to ensure the reliability of the new type connection and prevent the failure of No. 1, No. 3, and No. 4, the length and thickness of the steel plate hoop in the connection and the sectional area of the bolt should be designed.

4.2. The Bearing Capacity of Section 2-2. The section 2-2 is composed of steel tube and concrete, without reinforcement penetration, and it belongs to a typical rectangular steel tube concrete section. Therefore, it can be calculated according to the formula of medium-pressure bending members in the technical specification for structures with concrete-filled rectangular steel tube members [26], and the bearing capacity shall meet the following two formulas at the same time:

$$M_{\text{un}} = [0.5A_{\text{sn}}(h - 2t - d_n) + bt(t + d_n)]f, \tag{5}$$

$$\frac{M}{M_{\text{un}}} \leq \frac{1}{\gamma}, \tag{6}$$

$$\frac{N}{N_{\text{un}}} + (1 - \alpha_c)\frac{M}{M_{\text{un}}} \leq \frac{1}{\gamma}, \tag{7}$$

where M_{u1} is the flexural capacity of the column under the single bending moment, b and h are the length of the parallel bending axial and vertical bending axial, respectively, t is the thickness of the steel plate hoop, A_{sn} is the section area of steel pipe, d_n is height of concrete compression zone in steel pipe, f is the bending strength of steel plate, N_{un} is the compressive capacity of the column under the single axial pressure, α_c is concrete work bearing coefficient, and γ is the coefficient, which is taken as 0.8 according to the technical regulations.

4.3. The Bearing Capacity of Section 3-3. The section 3-3 can be calculated according to the bending and compression capacity of typical reinforced concrete. Its bearing capacity calculation formula is calculated according to the relevant formula in the code for design of concrete structures (GB50010-2010) [21].

1. The calculation of flexural and axial capacity is given as follows:

$$M_{\text{ub}} \leq \alpha_1 \text{f}_\text{c} \text{b} x\left(h_0 - \frac{x}{2}\right) + \text{f}'_\text{y}\,\text{A}'_\text{s}(h_0 - \alpha'_s), \tag{8}$$

where M_{ub} the flexural capacity of 2-2 section, α_1 is equivalent coefficient of concrete, f_c is strength of concrete, A'_s is

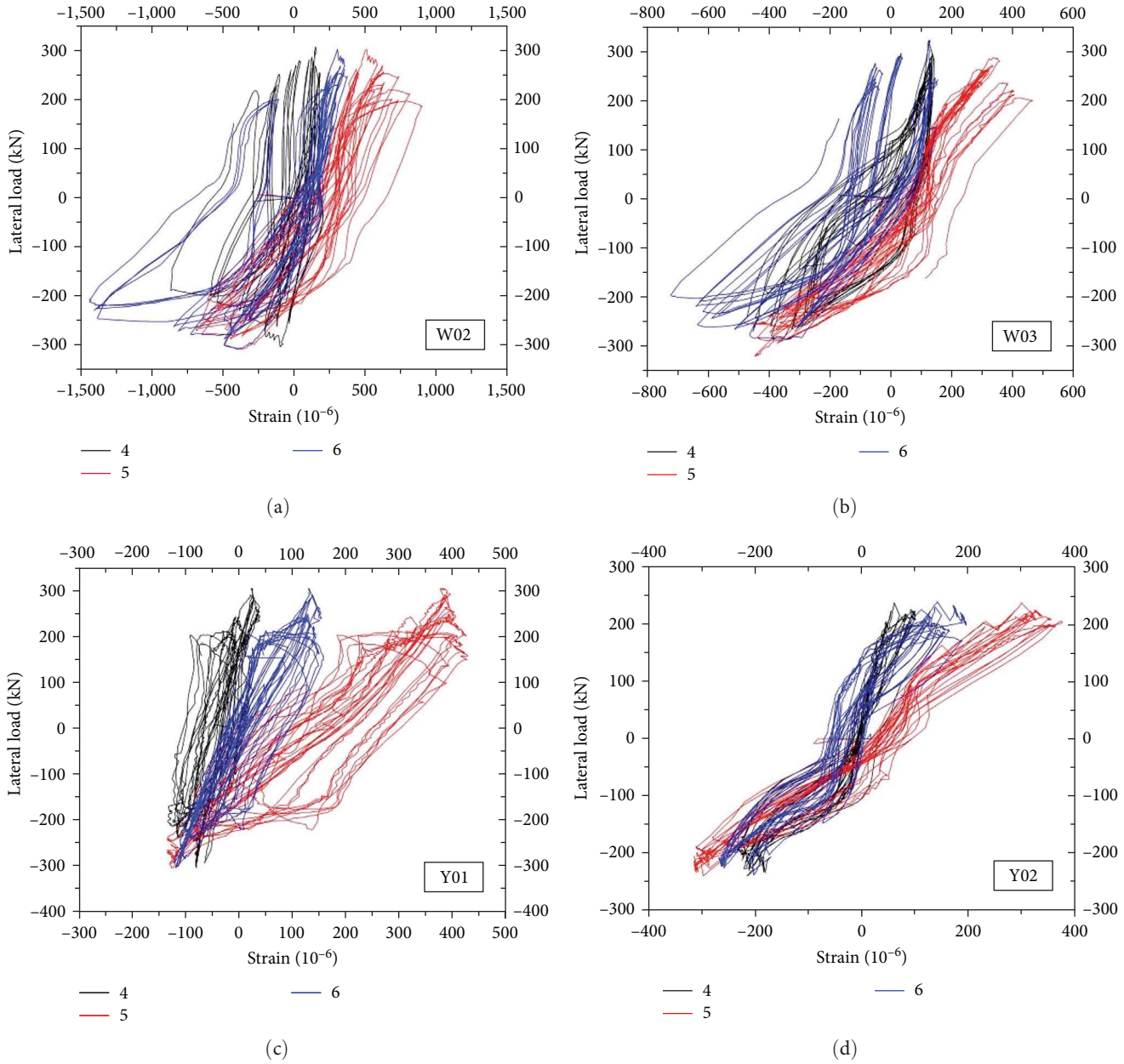

FIGURE 15: Strain curve of the steel hoop: (a) W02; (b) W03; (c) Y01; (d) Y02.

section area of longitudinal reinforcement in compression zone, h_0 is effective height of section, and α_s' is the distance from the resultant force point to the edge of the section.

2. The calculation of shear capacity is shown as follows:

$$V \geq \frac{1.75}{\lambda + 1} f_t b_c h_0 + \rho_{sv} f_{sv} b_c h_0 + 0.07N, \tag{9}$$

where V the shear capacity of 2-2 section, λ is the shear span ratio, f_t is tensile strength of concrete, f_{sv} is the tensile strength of stirrups, h_0 is effective height of section, and b_c is the section length of column.

4.4. The Shear Capacity of Bolts. In order to analyze the stress condition of the bolts, the process of force transmission in the new type connection can be analyzed, and each component is isolated separately to analyze its stress condition, as shown in Figure 18.

As shown in Figure 18(a), the stress equilibrium state of precast concrete member A is shown. According to the mechanical equilibrium equation, the following three formulas can be obtained:

$$\begin{aligned} \sum F_y = 0 &\longrightarrow N + F_{V7} + F_{V8} + \int_0^{L_{cd}} \\ \tau_{cd} b dx &= \int_0^h \sigma_{ce} b dx + F_{V7} + F_{V8} + \int_0^{L_{cf}} \\ \tau_{cf} b dx &\longrightarrow N = \int_0^h \sigma_{ce} b dx + \int_0^{L_{cf}} \tau_{cf} b dx - \int_0^{L_{cd}} \tau_{cd} b dx, \end{aligned} \tag{10}$$

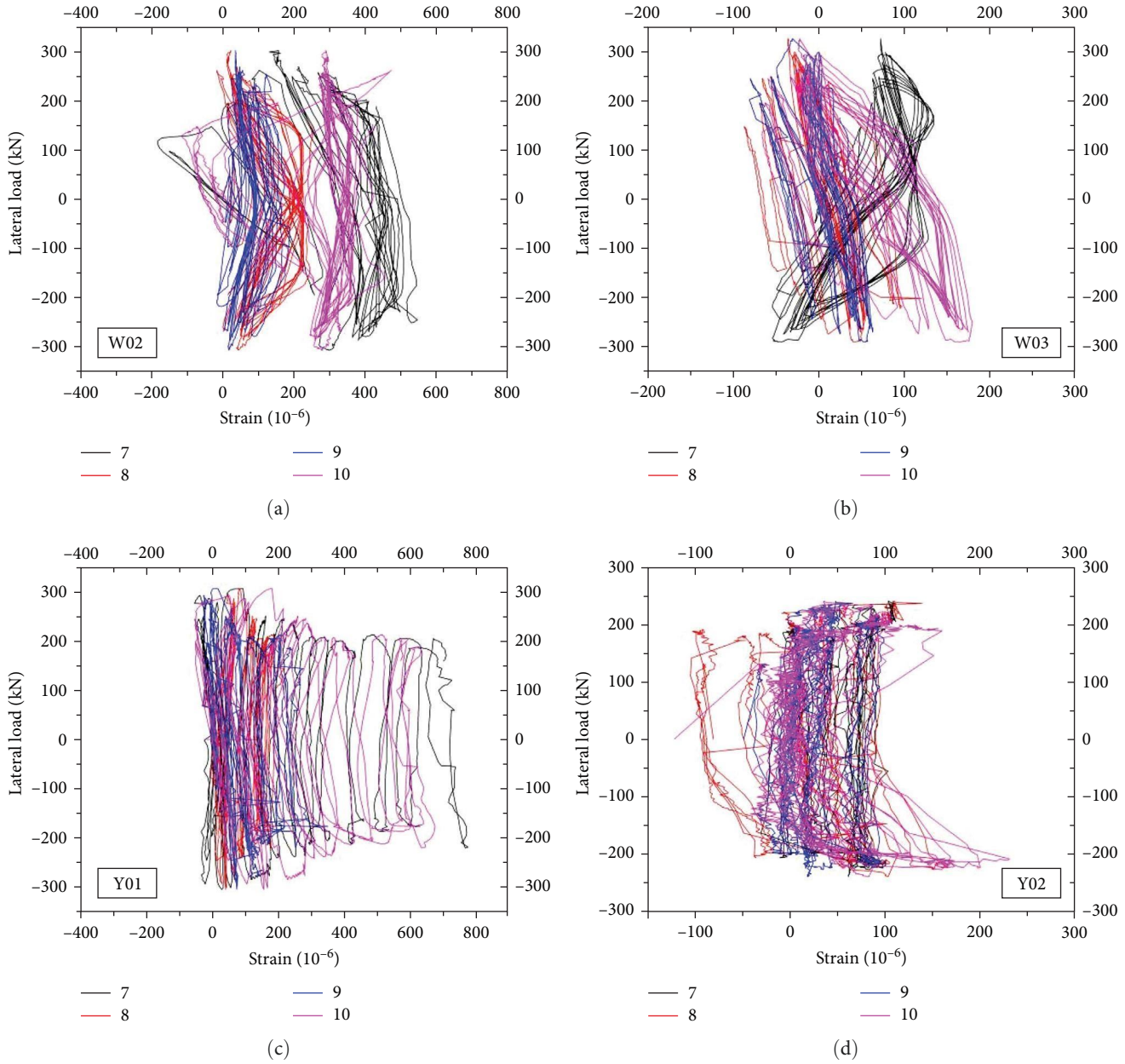

FIGURE 16: Load-strain curve of bolts: (a) W02; (b) W03; (c) Y01; (d) Y02.

$$\begin{aligned}
\sum F_x = 0 &\longrightarrow V + F_{N7} + F_{N8} + \int_0^{L_{cd}} \sigma_{cd} b dx = \int_0^{h} \tau_{ce} b dx + F_{N7} + F_{N8} + \int_0^{L_{cf}} \sigma_{cf} b dx \\
&\longrightarrow V + \int_0^{L_{cd}} \sigma_{cd} b dx + \int_0^{h} \tau_{ce} b dx = \int_0^{L_{cf}} \sigma_{cf} b dx, \\
\sum M_{C+} &= \sum M_{C-} \\
V \cdot \frac{L}{2} &+ \left(\int_0^{L_{cd}} \sigma_{cd} b dx \right) \cdot L' = \left(\int_0^{h} \sigma_{ce} b dx \right) \cdot h_0' \\
&+ \left(\int_0^{L_{cf}} \tau_{cf} b dx + \int_0^{L_{cd}} \tau_{cd} b dx \right) \cdot \frac{h}{2} \\
&+ \left(\int_0^{L_{cf}} \sigma_{cf} b dx \right) \cdot L'' + (F_{V7} + F_{V8}) \cdot h,
\end{aligned} \tag{11}$$

(12)

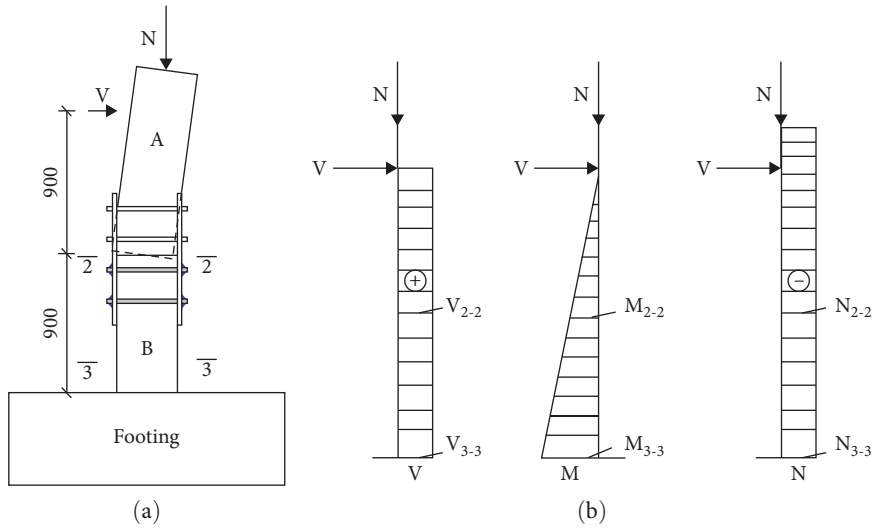

FIGURE 17: Internal force diagram of test columns: (a) deformation trend of the columns; (b) internal force diagram of the columns.

where σ_{cf}, σ_{cd}, σ_{cg}, and σ_{ch} are the compressive stresses between the steel plate hoop and the concrete members; τ_{cf}, τ_{cd}, τ_{cg}, and τ_{ch} are the shear stress between the concrete member and the steel plate hoop; F_{V7}, F_{V8}, F_{V9}, and F_{V10} are the shear forces borne by bolts No. 7, No. 8, No. 9, and No. 10, respectively; L'' is the distance from the acting point of σ_{cf} to the bottom edge; L' is the distance from the acting point of σ_{cd} resultant force to the bottom edge; and h_0' is the distance from the acting point of σ_{ce} resultant force to the bottom edge.

According to the stress situation, both l' and h_0' are far less than the value of l''. Therefore, in order to simplify the calculation, the relevant terms of the two values in the Formula 12 can be omitted. So, the relevant terms of the two values in the Formula 12 can be omitted. The value of τ_{cd} is close to τ_{cf}, so the two formulas can be combined into $2\tau_{cf}$, and the following Formula 11 can be obtained.

$$V \cdot \frac{\mathrm{L}}{2} = \left(\int_0^{L_{cf}} \tau_{cf} b dx \cdot h + \int_0^{L_{cf}} \sigma_{cf} b dx\right) \cdot L'' + (F_{V7} + F_{V8}) \cdot h. \tag{13}$$

According to the data provided in [27–29], and combined with the steel hoop and concrete materials in this test, the static friction coefficient between steel hoop and member is 0.2. Therefore, the relation formula between τ_{cf} and σ_{cf} can be obtained as $\tau_{cf} = 0.2\sigma_{cf}$. So, the Formula 14 can be obtained.

$$V \cdot \frac{\mathrm{L}}{2} = \int_0^{L_{cf}} \sigma_{cf} b dx \cdot (L'' + 0.2h) + (F_{V7} + F_{V8}) \cdot h. \tag{14}$$

Bringing Formula 11 into Formula 14, Formula 15 is obtained.

$$V \cdot \left(\frac{\mathrm{L}}{2} - L'' - 0.2h\right) = \left(\int_0^{L_{cd}} \sigma_{cd} b dx + \int_0^{h} \tau_{ce} b dx\right) \cdot (L'' + 0.2h) + (F_{V7} + F_{V8}) \cdot h. \tag{15}$$

The two items τ_{ce} and σ_{cd} can be ignored. The first reason is that τ_{ce} and σ_{cd} are small, and the second reason is that they can improve the safety of bolts. So, the Formula 14 can be obtained.

$$V \cdot \left(\frac{\mathrm{L}}{2} - L'' - 0.2h\right) = (F_{V7} + F_{V8}) \cdot h, \tag{16}$$

$$F_{V7} + F_{V8} = \frac{V \cdot \left(\frac{\mathrm{L}}{2} - L'' - 0.2h\right)}{h}, \tag{17}$$

$$A_{sv} = \frac{V \cdot \left(\frac{\mathrm{L}}{2} - L'' - 0.2h\right)}{f_{sv} h}, \tag{18}$$

where A_{sv} is the bolts section area, V is the lateral load, L is the distance from the lateral load to the bottom of column, h is the height of concrete column section, f_{sv} is the shear strength of the bolts, and L'' is the distance from the acting point of σ_{cf} to the bottom edge, and it is related to the length of steel plate hoop.

5. Analysis of Theoretical Analysis and Experimental Results

According to the above stress analysis, the calculation results are shown in Table 4. M_{un} is the bending capacity of section 2-2, which can be calculated according to Formula 5 [30]. M_{ub} is the flexural and axial capacity of section 3-3, which can be calculated according to Formula 8. V is the shear capacity of section 3-3, which can be calculated according to Formula 9. A_{sv} is the section area of bolts, which can be

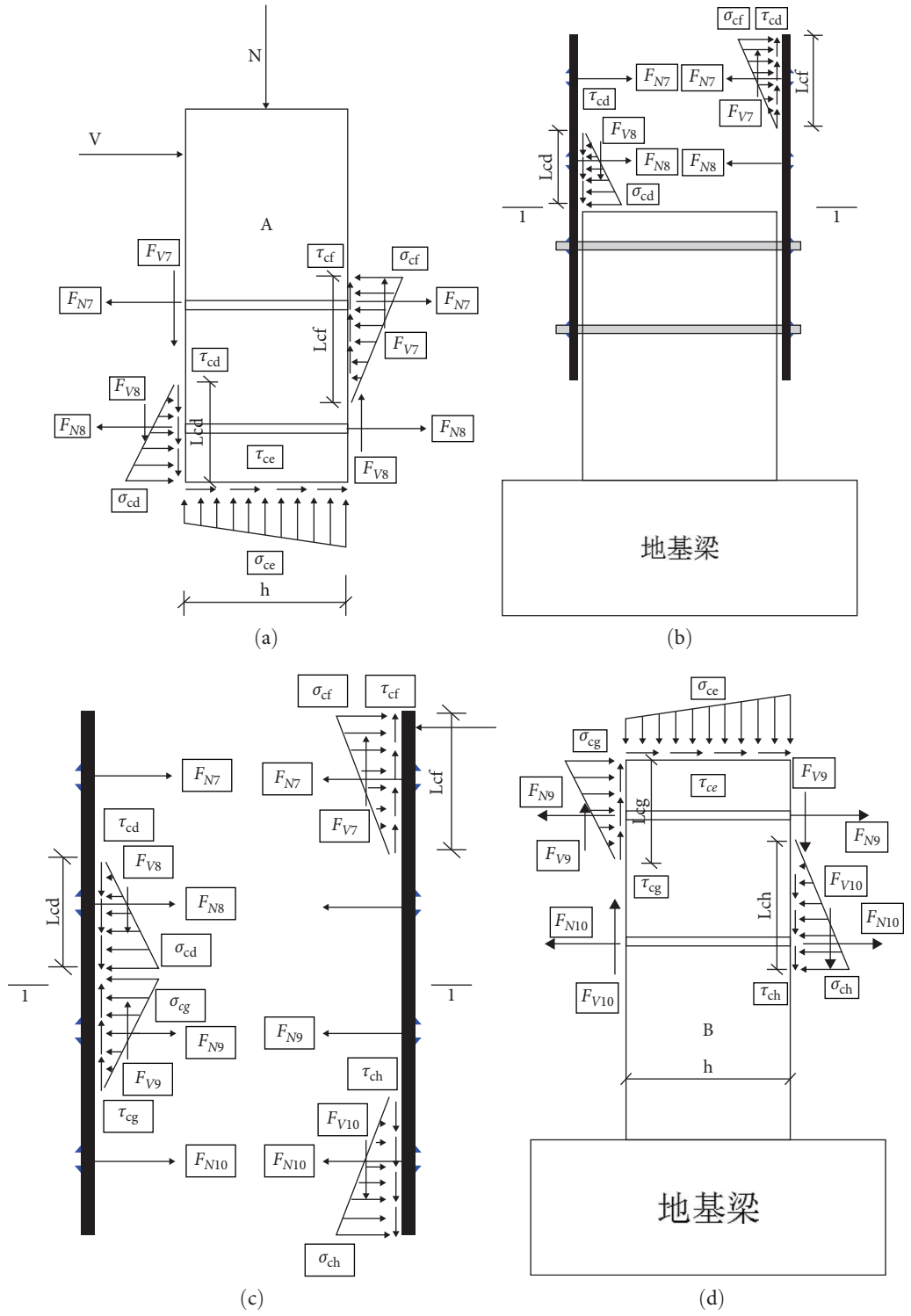

Figure 18: Stress diagram of each component: (a) stress conditon of prefabricated component A; (b) stress condition of lower part; (c) stress condition of steel tube; (d) stress conditon of prefabricated component B.

Table 4: Theoretical calculation results.

Specimen	M_{un} (kN·m)	M_{ub} (kN·m)	M' (kN·m)	V (kN)	A_{sv} (mm^2)
W01		655.7	695.3	502.2 (326.6)	
W02	472.0 (329.6)	655.7	659.1	502.2 (307.2)	1,017.5 (1,519.76)
W03	565.0 (342.1)	655.7	684.2	502.2 (325.2)	1,017.5 (1,519.76)
Y01	472.0 (330.3)	655.7	660.5	502.2 (305.9)	1,235.3 (1,519.76)

calculated according to Formula 18. The data in brackets are the actual test values.

M', as shown in Table 4, is the actual bending moment of the columns, and it can be calculated according to Formula 19.

$$M' = Ne + VL, \tag{19}$$

where N is the axial pressure of the column, e is the lateral displacement, V is the horizontal force, L is the length from the lateral force to the column bottom, Ne is the bending moment generated by eccentric action, and VL is the bending moment generated by horizontal shear.

As shown in Table 4, the M' is greater than M_{ub}, and the other calculated values of M_{un}, V, and A_{sv} are all greater than the test values. This shows that all test columns will occur bending failure at section 3-3, and other failure forms will not occur, which is is consistent with the test results.

6. Conclusion

This paper presents an experimental investigation on the seismic performance of a fabricated connection columns with steel plate hoop and bolts. Four fabricated columns and two cast-in-situ columns were tested while subjected to combined axial compression and cyclic lateral loading. Based on the discussion of the test results, the following conclusions can be made:

(1) The hysteresis curves of the new type connection columns were plump and the pinch phenomenon was not obvious. The interlayer displacement of all test pieces was greater than 1/50, the displacement ductility ratio of the fabricated columns was between 2.5 and 5.0, and the overall strength attenuation coefficient was above 0.8. The prefabricated columns were slightly higher than the cast-in-situ columns, and the stiffness attenuation coefficient of prefabricated columns was almost the same as the cast-in-situ columns. In general, the new type column-to-column connection was equivalent to the cast-in-situ connection, which can provide reference for the application of prefabricated concrete frame structure in the earthquake area.

(2) The strain curves at the locations, including longitudinal reinforcements, stirrups, steel plate hoops, and bolts, were analyzed. The main function of the steel plate hoop in the new type connection was to transmit the bending moment, and the tensile force of the longitudinal reinforcement in the upper precast concrete member was transmitted to the lower member through bolts and steel plate hoops [31]. Since the connection point was not at the maximum bending moment in this test, no yield deformation of the steel plate hoops and bolts was observed, which was consistent with the design result.

(3) The mechanical transmission mode of the new type connection was analyzed. The formula for calculating the bearing capacity of the connection was given, including the minimum thickness of the steel plate hoop, the length of the steel plate hoop, and the section area of bolts. The rationality of the calculation formula was verified by comparing the test results and the calculation results.

(4) The shear mechanism of this new type connection is still unclear, and there is a lack of necessary shear capacity test data and results. Therefore, the conditions for this connection model to be applied to prefabricated concrete beam-to-beam connections are not enough.

Data Availability

The authors confirm that the data supporting the findings of this study are available within the article materials.

Conflicts of Interest

The authors declare that they have no conflicts of interest.

Acknowledgments

The authors acknowledge the National Science Foundation of China Project 51408453 and the General program of Shaanxi Natural Science Foundation 2023-JC-YB-373, 2020JM-475.

References

[1] D. Mitchell, R. H. DeVall, M. Saatcioglu, R. Simpson, R. Tinawi, and R. Tremblay, "Damage to concrete structures due to the 1994 Northridge earthquake," *Canadian Journal of Civil Engineering*, vol. 22, no. 2, pp. 361–377, 1995.

[2] Civil Engineering Structure Expert Group, "Seismic damage analysis of buildings in Wenchuan earthquake," *Journal of Building Structures*, vol. 29, no. 4, pp. 1–9, 2008.

[3] S. Ozden, E. Akpinar, H. Erdogan, and H. M. Atalay, "Performance of precast concrete structures in October 2011 Van earthquake, Turkey," *Magazine of Concrete Research*, vol. 66, no. 11, pp. 543–552, 2014.

[4] M. J. Nigel Priestley, "The PRESSS program current status and proposed plans for phase III," *PCI Journal*, vol. 41, no. 2, pp. 22–40, 1996.

[5] X. K. Huang, C. Y. Tian, M. L. Wan, and R. Li, "Researches and applications of precast concrete structures in China," *China Building Science*, vol. 34, no. 9, pp. 53–58, 2018.

[6] S. Mao, B. Sun, and J. Qi, "Review of research on connection technology of precast concrete structure," *Construction Technology*, vol. 51, no. 11, pp. 49–63, 2022.

[7] Y. Zheng, "*Research on rebar splicing system by GDPS grout-filled coupling sleeve*," Doctoral thesis, Southeast University, Nan Jing, China, 2016.

[8] C. Han, Y. Zheng, and Y. Zhao, "Research and appHcation deVelopment of grout sleeVe splicing for reinforcement," *Construction Technology*, vol. 42, no. 21, pp. 113–116, 2013.

[9] M. Wei and X. Fang, "Tests on behavior of precast columns with reinforcements spliced," *Journal of Jiamusi University (Natural Science Edition)*, vol. 31, no. 3, pp. 352–361, 2013.

[10] N. Tullini and F. Minghini, "Grouted sleeve connections used in precast reinforced concrete construction—experimental

investigation of a column-to-column joint," *Engineering Structures*, vol. 127, pp. 784–803, 2016.
[11] R. Li, Y. M. Zheng, and Y. Zhao, "Experimental research on seismic columns with 500 1VIPa reinforcements splicing performance of precast concrete by grout-filled coupling sleeves," *Journal of Building Structures*, vol. 37, no. 5, pp. 255–263, 2016.
[12] J. Wang, J. Zhao, and Z. Hu, "Review and thinking on development of building industrialization in China," *China Civil Engineering Journal*, vol. 49, no. 5, pp. 1–8, 2016.
[13] Y. Chen, "Common quality problems and preventive measures in precast concrete building construction," *Technology and Market*, vol. 26, no. 5, pp. 197–199, 2019.
[14] T. Ding, J. Xiao, Q. Zhang, and A. Akbarnezhad, "Experimental and numerical studies on design for deconstruction concrete connections: an overview," *Advances in Structural Engineering*, vol. 21, no. 14, pp. 2198–2214, 2018.
[15] S. A. Kulkarni and L. Bing, "Investigations of seismic behavior of hybrid connections," *PCI Journal*, vol. 54, no. 1, pp. 67–87, 2009.
[16] G. Metelli and P. Riva, "Behaviour of a beam to column "dry" joint for precast concrete elements," in *14th World Conference on Earthquake Engineering*, WCEE, 2008.
[17] Y. Yang and L. Han, "Experimental research on the flexural mechanical properties of rectangular steel tube concrete members," *Earthquake Engineering and Engineering*, vol. 21, no. 3, Article ID 8, 2001.
[18] GB/T50081-2019, "Standard for test method of mechanical," 2019.
[19] GB/T 50081-2002, "Standard for test method of mechanical properties on ordinary concrete," 2002.
[20] JGJ/T 101-2015, *Specification for Seismic Test of Buildings*, China Architecture & Building Press, Beijing, 2015.
[21] GB 50011-2010, *Code for Seismic Design of Buildings*, China Architecture & Building Press, Beijing, 2010.
[22] W. Yan, W. Wang, and S. Chen, "Experimental study of the seismic behavior of precast concrete layered slab and beam to column exterior joints," *China Civil Engineering Journal*, vol. 43, no. 12, pp. 56–61, 2010.
[23] W. Li, L. Sun, J. Zhao, P. Lu, and F. Yang, "Seismic performance of reinforced concrete columns confined with two layers of stirrups," *The Structural Design of Tall and Special Buildings*, vol. 27, no. 12, Article ID e1484, 2018.
[24] L. Sun and W. Li, "Cyclic behavior of reinforced concrete columns confined with two layers of stirrups," *Structural Concrete*, vol. 20, no. 4, pp. 1279–1291, 2019.
[25] CECS 159:2018, "Technical specification for structures with concrete-filled rectangular steel tube member," (in Chinese), 2018.
[26] X. L. Kang, H. T. Zhao, J. Y. Xue, and Z. Chen, "Summarized review of the bond slip problems of concrete filled steel tubes," *Journal of Xi'an University of Architecture & Technology*, vol. 38, no. 3, pp. 321–326, 2006.
[27] L. Han, *Concrete Filled Steel Tube*, Science Press, 2000.
[28] S. Li, Q. Li, H. Jiang, H. Zhang, and L. Zhang, "Experimental research on seismic performance of a new-type of R/C beam-column joints with end plates," *Shock and Vibration*, vol. 2017, Article ID 3823469, 11 pages, 2017.
[29] L. Zeng, *Research on Seismic Behaviors and Design Method of Steel Reinforced High Strength and High Performance Concrete Frame Joints*, Xi'an University of Architecture and Technology, Xi'an, China, 2008.
[30] S. Al-Obaidi, T. Salim, and S. A. Hemzah, "Flexural behavior of concrete filled steel tube composite with different concrete compressive strength," *International Journal of Civil Engineering and Technology*, vol. 9, no. 7, pp. 824–832, 2018.
[31] D. Yuan, Q. Li, J. Sun, J. Zhang, and W. Jiang, "Three-point bending behaviour of a fabricated concrete connection with steel plate hoop and bolts," *Advances in Civil Engineering*, vol. 2021, Article ID 5589668, 17 pages, 2021.